Efficient production of 100 keV deuterons in deuterium gas puff Z-pinches at 2 MA current

2010 Plasma Phys. Control. Fusion 52 065013

(http://iopscience.iop.org/0741-3335/52/6/065013)

Plasma Phys. Control. Fusion **52** (2010) 065013 (17pp) doi:10.1088/0741-3335/52/6/065013

Efficient production of 100 keV deuterons in deuterium gas puff Z-pinches at 2 MA current

D Klir[1], J Kravarik[1], P Kubes[1], K Rezac[1], J Cikhardt[1], E Litseva[1], T Hyhlik[2], S S Ananev[3], Yu L Bakshaev[3], V A Bryzgunov[3], A S Chernenko[3], Yu G Kalinin[3], E D Kazakov[3], V D Korolev[3], G I Ustroev[3], A A Zelenin[3], L Juha[4], J Krasa[4], A Velyhan[4], L Vysin[4], J Sonsky[5] and I V Volobuev[6]

[1] Czech Technical University in Prague, Faculty of Electrical Engineering, Department of Physics, Technicka 2, 166 27 Prague 6, Czech Republic
[2] Czech Technical University, Faculty of Mechanical Engineering, Department of Fluid Dynamics and Power Engineering, Technicka 4, 166 27 Prague, Czech Republic
[3] Institute of Nuclear Synthesis, RRC Kurchatov Institute, 1 Kurchatov Sq., 123182 Moscow, Russia
[4] Institute of Physics, Academy of Sciences of the Czech Republic, Na Slovance 2, 182 21 Prague 8, Czech Republic
[5] Institute of Thermomechanics, Academy of Sciences of the Czech Republic, Dolejskova 5, 182 00 Praha 8, Czech Republic
[6] P.N. Lebedev Physical Institute, Russian Academy of Sciences, Leninsky prospect 53, 119991 Moscow, Russia

E-mail: klirdani@fel.cvut.cz

Received 11 March 2010, in final form 28 April 2010
Published 12 May 2010
Online at stacks.iop.org/PPCF/52/065013

Abstract

Deuterium gas puff experiments were carried out on the S-300 Z-pinch at the Kurchatov Institute in Moscow. Gas puffs imploded onto the axis before a current peak at about 100 ns. Fusion neutrons were generated after the gas puff implosion during global expansion of a plasma column. Neutron emission lasted on average 35 $\pm$ 5 ns (full width half maximum, FWHM). In the downstream direction (on the Z-pinch axis behind the cathode), a mean neutron energy was 2.6 $\pm$ 0.1 MeV. Side-on neutron energy spectra peaked at 2.40 $\pm$ 0.05 MeV with about 600 $\pm$ 150 keV FWHM. A broad width of side-on neutron spectra implied a high radial component of deuteron velocities. An average kinetic energy of fast deuterons, which produced fusion neutrons, was 150 keV. A peak neutron yield reached a value of 6×10^{10} on a current level of 1.5 MA. It was by one order higher in comparison with other deuterated loads used on the same current generator. On the basis of experimental observations, we concluded that a total energy of deuterons accelerated to fusion energies was above 1.5 kJ. It is more than 15% of the energy input into a plasma. Therefore gas puff Z-pinches seem to be not only powerful sources of x-ray radiation but also efficient sources of 100 keV deuterons. Such a result is consistent with high

neutron yields observed on the Angara Z-pinch and plasma foci with similar currents.

(Some figures in this article are in colour only in the electronic version)

1. Introduction

The first systematic study of Z-pinches started in the 1950s in connection with controlled thermonuclear fusion research. Straight compressional Z-pinches were found to produce a large number of neutrons which originated from the D(d,n)^{3}He fusion reaction [1–3]. Shortly afterwards, researchers arrived at the conclusion that neutrons were not of thermonuclear origin and that straight Z-pinches were not useful for fusion power production. Nevertheless, a large number of produced neutrons in Z-pinches led to the study of acceleration of deuterons to fusion energies. In order to cope with this reality satisfactorily and to achieve even higher neutron yields, various configurations based on the Z-pinch effect have been suggested and tested from that time on. The most promising configuration seemed to be a plasma focus with a deuterium gas filling (a record yield exceeded 10^{12} neutrons/shot on a megaampere current level [4]). In plasma foci (PF), many experimental results have been obtained and also neutron production mechanisms have been studied up to the present time [5–8]. In this respect, experimental data from Z-pinches are rather rare. One of those few examples is a Z-pinch which is formed from a frozen deuterium fibre or a deuterated plastic fibre. The first fibre Z-pinches in the 1980s seemed to be promising due to enhanced stability of plasma [9]. However, the enhanced stability was not confirmed in further and better diagnosed experiments and, in addition to that, peak neutron yields did not exceed 10^{10} with a megaampere current [10–13]. When a higher neutron yield was required, solid fibres appeared to be less suitable than a deuterium gas.

The first deuterium gas puff experiment was carried out on the Angara 5-1 Z-pinch at Troitsk at the end of the 1980s [14, 15]. Characteristic features of a solid deuterium gas puff were the axial gradient of a linear density $\mathrm{d}N/\mathrm{d}z \approx 10^{18}\,\mathrm{cm}^{-2}$ and a relatively small mass of a deuterium gas near the anode. This way, more than 10^{12} neutrons were emitted within 50 ns at a current of 'only' 2 MA. Neutron energy spectra gave evidence of deuterons accelerated to 200–500 keV energies.

A few years later, a hollow deuterium gas puff Z-pinch was researched on the Saturn generator [16]. Even though the current was higher (about 7–9 MA), a peak neutron yield of about 2×10^{12} was comparable to that achieved on the Angara. We should perhaps comment here on the fact that the saturation of a neutron yield at the value of 10^{12} has been also observed during plasma focus research and this was one of the most important arguments for shutting down the largest plasma focus facilities. In this respect, 4×10^{13} neutrons from a double-shell D_2 gas puff on the 17 MA Z-machine in 2005 seemed to be a crucial finding [17–19]. In addition to that, MHD [19] and particle-in-cell [20] simulations showed that there is a hope of a large thermonuclear component. Higher ratio between thermonuclear and beam–target neutrons could also explain the overcoming of the saturation at 10^{12} neutrons/shot.

Since 2007 we have carried out deuterium gas puff experiments on the S-300 generator at the Kurchatov Institute. The first reason for our experiments is our interest in the study of the neutron production mechanism. The second reason is to learn more about fast deuterons because the information about ions in Z-pinches is rather rare. Since neutrons are influenced neither by magnetic nor by electric fields, the detection of neutrons is a favourable diagnostic

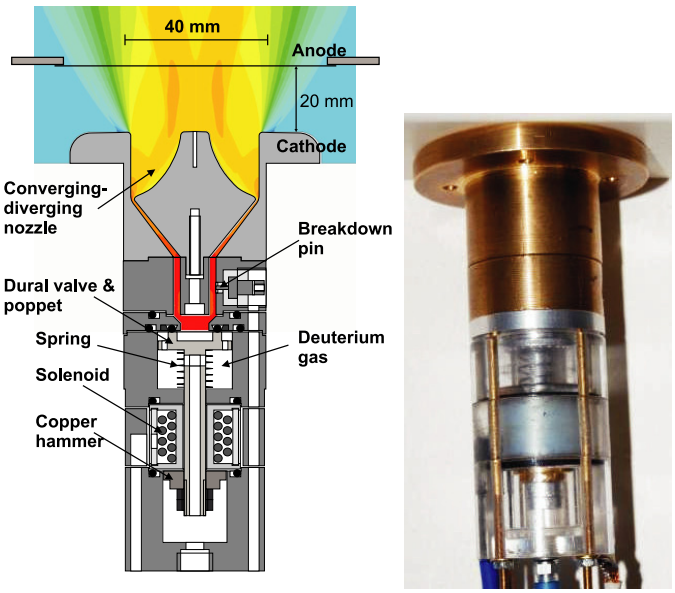

Figure 1. Electromagnetic valve.

Table 1. Parameters of electromagnetic valve.

Inductance of solenoid	$L = 2.5\,\mu$H
Capacitance	$C = 200\,\mu$F
Charging voltage	$V = 1.6$–2.8 kV
Current (at 2.6 kV)	$I_{\max} = 17$ kA
Opening speed of the poppet (at 17 kA)	$v = 3\,\mathrm{m\,s^{-1}}$
Deuterium pressure	$p = 1$–4 bar
Voltage at breakdown pin	$V_{\mathrm{PIN}} = 400$–1000 V
Initiation of the current generator after the breakdown pin pulse	$t = 150$–$1000\,\mu$s

tool for fast deuterons in a plasma. The third reason is to perform deuterium gas puff experiments on a 1–2 MA level, i.e. with a comparable current as in experiments on the Angara and on the largest plasma focus devices PF-1000 [21] and PF-3 [22]. Not only do we intend to repeat successful results achieved on the Angara, but we would also like to provide more experimental data from a deuterium gas puff Z-pinch by means of a comprehensive set of neutron and x-ray diagnostics. Last but not least, our experiments make it possible to enlarge the neutron scaling law for deuterium gas puffs below 2 MA currents.

In our preliminary gas puff experiments at the S-300 [23], the gas puff was driven by burning gun powder similarly as at Troitsk on the Angara. However, in our experiments, the deuterium gas was likely interfused with the burning gun powder and thus a mass density was too high (above $200\,\mu\mathrm{g\,cm^{-1}}$). In this paper, we present results from experiments with the linear mass density of about $20\,\mu\mathrm{g\,cm^{-1}}$ which was achieved with a new electromagnetic valve. The construction of this valve, an experimental arrangement and diagnostics used in our experiment are described in section 2. Section 3 provides the most important experimental results. The discussion of these results is the subject of section 4. Finally, section 5 brings an overall summary.

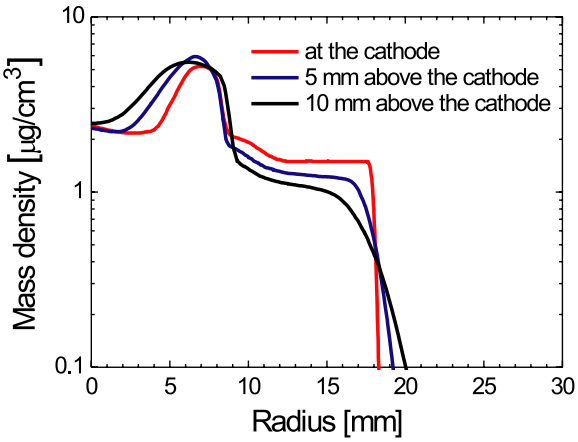

Figure 2. Simulated mass density profiles at various distances above the cathode in the case of a 20 μg cm^{-1} linear mass density.

2. Experimental arrangement and diagnostics

2.1. Experimental setup

The experimental series of 11 shots with a deuterium gas puff was carried out on the S-300 pulsed power generator (4 MA peak current, 700 kV voltage, 100 ns rise time, 0.15 Ω impedance [24, 25]) at the Kurchatov Institute (Moscow) in September 2009. The peak current in these shots varied between 1.4 and 1.7 MA. For the last experimental campaign, we constructed the electromagnetic valve the schematic diagram of which is displayed in figure 1. Parameters of the electromagnetic valve are displayed in table 1. By means of a fast optical framing camera, we measured a modest opening speed of the valve of 3 m s^{-1}.

As regards the design of a supersonic nozzle, we aim at testing various nozzles for both annular and solid gas puffs. We started with a convergent–divergent de Laval nozzle displayed in figure 1. When we calculated the steady state with the ANSYS FLUENT flow modelling software, we received the Mach number of about 6 and the linear density up to 50 μg cm^{-1} at 4 bar plenum pressure. At the initiation of the current generator, the plenum pressure significantly decreased. Therefore we calculated the linear mass density from observed implosion velocities and implosion time. In this paper, we present lower mass shots with the linear density of about 20 μg cm^{-1}. Calculated density profiles at various distances above the cathode can be seen in figure 2. The separation between the cathode and the anode was 11 or 20 mm.

2.2. Diagnostics

In order to study dynamics of the deuterium gas puff Z-pinch, we applied optical, x-ray and neutron diagnostics, part of which has already been described in more detail in [23, 26]. Each shot was observed with the following set of diagnostic tools (see also figure 3):

(i) A high-voltage probe (resistive divider) located at a radial distance of 2 cm [27].
(ii) $\mathrm{d}I/\mathrm{d}t$ probes placed at a 6.8 cm radius. From the differential equation $\dot{L}I = V - L\dot{I}$, we could numerically calculate the inductance $L(t)$ during the implosion when the resistive voltage RI is assumed to be negligible (for more details see [28]). Further, it was possible

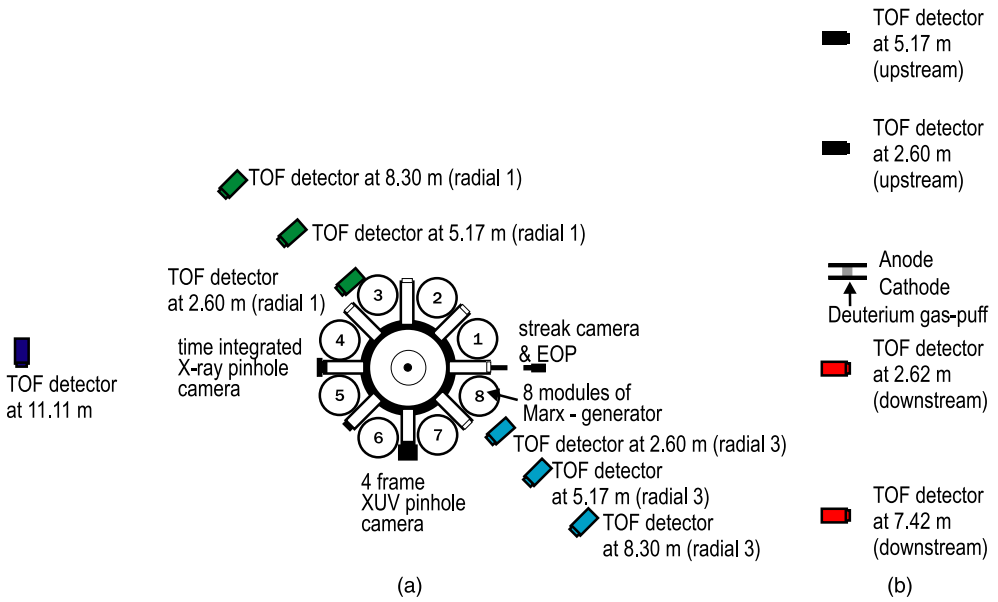

Figure 3. Schematic diagram of diagnostic setup with 11 TOF neutron detectors. (*a*) End-on view, (*b*) side-on view.

to evaluate the $\dot{L}I$ voltage and the active energy input into a plasma during the implosion $W_{\text{input}} = \int_0^{t_{\text{imp}}} VI\,\mathrm{d}t - \Delta(\frac{1}{2}LI^2) = \frac{1}{2}\int_0^{t_{\text{imp}}} \dot{L}I^2\mathrm{d}t$.

(iii) A radial optical streak camera. The plasma 5 mm above the cathode was imaged on the slit of the streak camera.

(iv) A 6-frame optical camera with 1 ns exposure and 10 ns inter-frame separation.

(v) A 3-fast-frame optical camera with 0.5 ns exposure and 0.9–1.0 ns inter-frame separation.

(vi) A 4-frame XUV pinhole camera with 2 ns exposure and 5 or 10 ns inter-frame separation.

(vii) A time-integrated x-ray pinhole camera (differentially filtered with 10 μm aluminium foil, 5 μm Mylar and 12 μm Mylar).

(viii) Two calibrated AXUV-5 semiconductor diodes with 36 μm and 121 μm Mylar filters.

(ix) Indium and silver activation counters located axially at 1 m above the anode.

(x) Thermoluminescent dosimeters (TLDs) placed inside a 10 inch thick Bonner sphere, 1 m from the neutron source (cf [29]).

(xi) Eleven hard x-ray and neutron time-of-flight (TOF) detectors based on a fast plastic scintillator (BC408 or its equivalent) and photomultiplier tube combination. Four axial (end–on) neutron detectors were located at distances of −5.17 m, −2.6 m (the minus sign stands for upstream, i.e. behind the anode), 2.6 m and 7.42 m (downstream, behind the cathode). Six radial (side-on) detectors were positioned in a row at distances of −8.3 m, −5.17 m, −2.6 m, 2.6 m, 5.17 m, 8.3 m from the Z-pinch plasma. One TOF detector was placed at 11.11 m, i.e. at the most distant place in the experimental hall. For preventing hard x-rays from saturating photomultipliers, detectors were shielded by 1–10 cm of lead. Neutron TOF diagnostics was used to give an insight into the acceleration of fast deuterons. The emphasis was put on finding more about the energy distribution of deuterons which produced fusion neutrons, about anisotropy of neutron emission and about the time and duration of neutron production with respect to general Z-pinch dynamics. A temporal resolution of neutron detectors was about 5 ns. The full width at half maximum

(FWHM) of neutron signals was more than 20 ns; therefore the 5 ns temporal resolution could not seriously affect neutron energy spectra reconstruction by the Monte Carlo simulation [30, 31]. Since hard x-ray and neutron signals were recorded on the same waveform and they were separated only by the TOF, the temporal uncertainty between hard x-rays and neutrons was on the order of the temporal resolution of a neutron detector. More details about our neutron diagnostics and Monte Carlo reconstruction of neutron energy spectra can be found in [23, 26].

This comprehensive set of diagnostic tools enabled us to achieve results that are described in the following section.

3. Experimental results

3.1. Plasma dynamics

During the experimental campaign in 2009, we carried out 11 shots with a linear mass density of $20\,\mu\mathrm{g\,cm^{-1}}$. Typical waveforms obtained in shot No 090930-2 with the deuterium gas puff Z-pinch are displayed in figure 4. The time described in this figure refers to the start of a current when $t = 0$.

In the case of $20\,\mu\mathrm{g\,cm^{-1}}$, the gas puff imploded onto the axis before the current peak at about 100 ns. An implosion velocity exceeded the value of $3 \times 10^5\,\mathrm{m\,s^{-1}}$. The implosion recorded by visible and XUV imaging seemed to be with a <10 ns zipper and with a diameter during the stagnation of about 2 mm (see also images in figure 5). The peak power of soft (>1.5 keV) x-rays was 70 MW with a total emitted energy of 2 J. It was a negligible fraction of the total energy input into a plasma $W_{\mathrm{input}} = \frac{1}{2}\int_0^{t_{\mathrm{imp}}} \dot{L} I^2 \mathrm{d}t$ which approached 9 kJ. Measured load impedances were consistent with the observed implosion velocities. The peak plasma impedance reached 0.30–0.45 Ω before the stagnation.

3.2. Hard x–ray and neutron production

Figure 4(*b*) shows waveforms of hard x-rays and neutrons recorded in the same shot as in figure 4(*a*). All signals were adjusted to account for different transit times from each detector to the oscilloscopes. The time of neutron production was estimated from the nearest side-on TOF detectors at 2.6 m from the Z-pinch plasmas. We shifted the observed neutron signals by 118 ns, i.e. by the TOF of 2.45 MeV neutrons. Therefore the temporal resolution of neutron detection was given by the width of a neutron energy spectrum and was experimentally estimated as 10 ns.

As regards the neutron emission in figure 4(*b*), there was a small neutron pulse which started during the stagnation and correlated with a hard x-ray peak. However, it was usually possible to distinguish two neutron pulses and the main emission (the second neutron pulse) corresponded to a small x-ray and hard x-ray peak. In all shots, the neutron emission started immediately after the maximum of $\dot{L} I$ voltage but it reached the peak 35 ns later. The neutron emission lasted for a quite long period with a 35 ± 5 ns FWHM. At this time, we did not observe any significant voltage peak and also the x-ray emission detected by silicon diodes was quite low. During the neutron emission, visible and XUV imaging recorded only a bright spot at the cathode whereas the streak camera showed the plasma expansion.

The total number of neutrons measured by the indium and silver activation counters in shot No 090930-2 was 2.6×10^{10} and 2.9×10^{10}, respectively. TLDs showed the neutron yield on the order of 10^{10}. The average neutron yield in all 11 shots was 3.5×10^{10} while the peak number of fusion neutrons in one shot approached 6×10^{10} at the maximum current of 1.3 MA. In comparison with previous experiments on the S-300, the yield is by one order

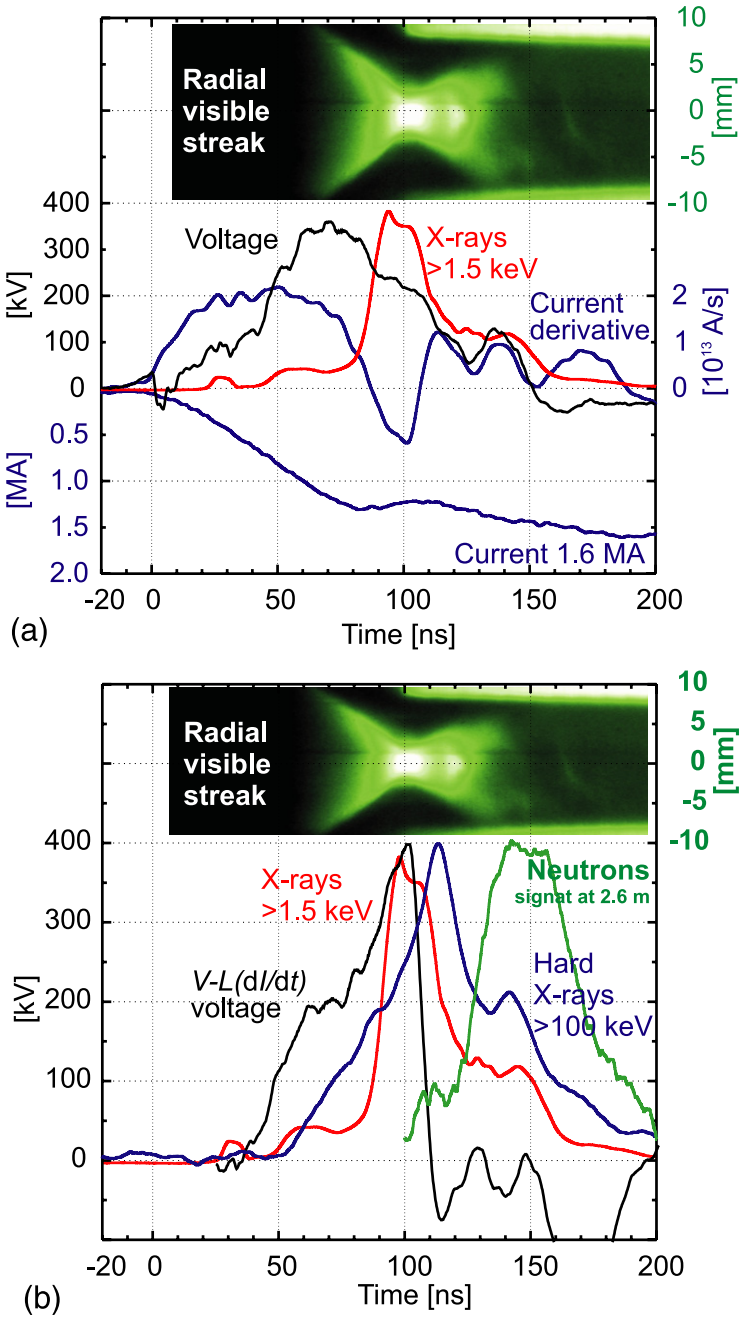

Figure 4. Discharge No 090930-2, the linear mass density of $20\,\mu g\,cm^{-1}$, the neutron yield of 3×10^{10}. (*a*) A visible streak image and waveforms of current, current derivative, voltage and x-rays. (*b*) A visible streak image and waveforms of $\dot{L}I$ voltage, x-ray, hard x-ray and neutron signals.

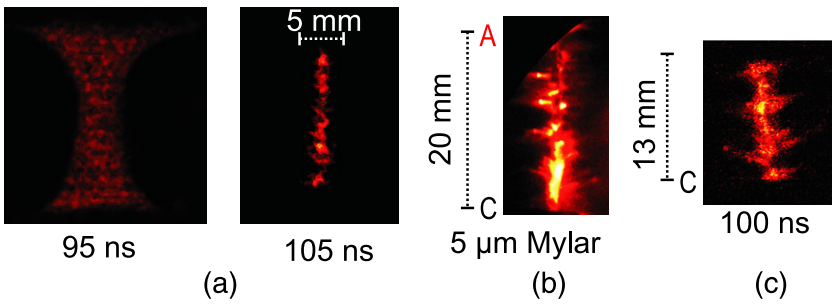

Figure 5. An example of images achieved with the deuterium gas puff. (*a*) Visible frames, shot No 090930-1, neutron yield of 4.5×10^{10}. (*b*) Time-integrated x-ray pinhole image, shot No 090928-1, neutron yield of 2×10^{10}. (*c*) XUV pinhole image, shot No 090930-2, neutron yield of 3×10^{10}.

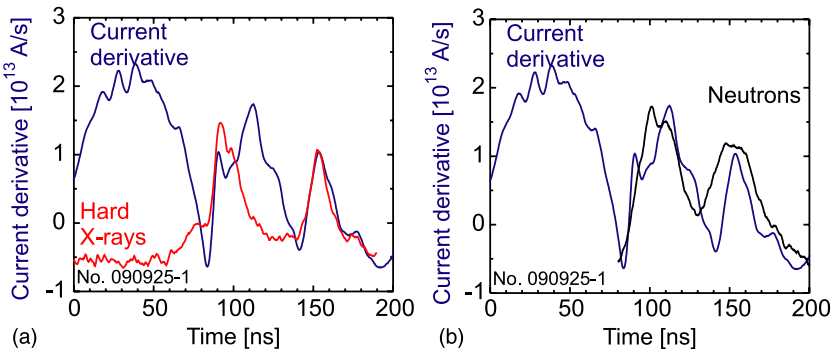

Figure 6. An example of the correlation of the $\mathrm{d}I/\mathrm{d}t$ signal with hard x-ray and neutron emission detected at the side-on detector at 2.6 m. The neutron signal was shifted by the TOF of 2.45 MeV neutrons. Shot No 090925, neutron yield of 3×10^{10}. (*a*) $\mathrm{d}I/\mathrm{d}t$ signal and hard x-rays. (*b*) $\mathrm{d}I/\mathrm{d}t$ signal and neutrons.

higher than the one with deuterated fibres [26, 32], X-pinches, deuterated foams [33, 34] and imploding wire-arrays [26].

3.3. Correlation of neutron and hard x-ray emission with $\mathrm{d}I/\mathrm{d}t$ *signal*

Temporal correlations of neutron and hard x-ray emission with electrical characteristics were investigated because we believe that it could throw more light on the process of accelerating charged particles. A common feature of our experiment was the correlation of hard x-rays with the signal of the $\mathrm{d}I/\mathrm{d}t$ probe. The most exemplary result was observed in the shot with one additional neutron pulse at 150 ns (cf figure 6). In all shots, the rapid increase of hard x-rays started immediately after the dip in the $\mathrm{d}I/\mathrm{d}t$ signal. Further, it was clear that the maxima of hard x-rays corresponded to the $\mathrm{d}I/\mathrm{d}t$ peaks. The current increase caused by these $\mathrm{d}I/\mathrm{d}t$ peaks was 100–200 kA.

Similar correlations were observed also in the case of neutron emission. However, neutrons were usually a little delayed which could be ascribed (i) to the time separation between deuteron acceleration and neutron production, (ii) to the transit time of neutrons through the TOF detector and (iii) to the uncertainty of neutron energy estimation.

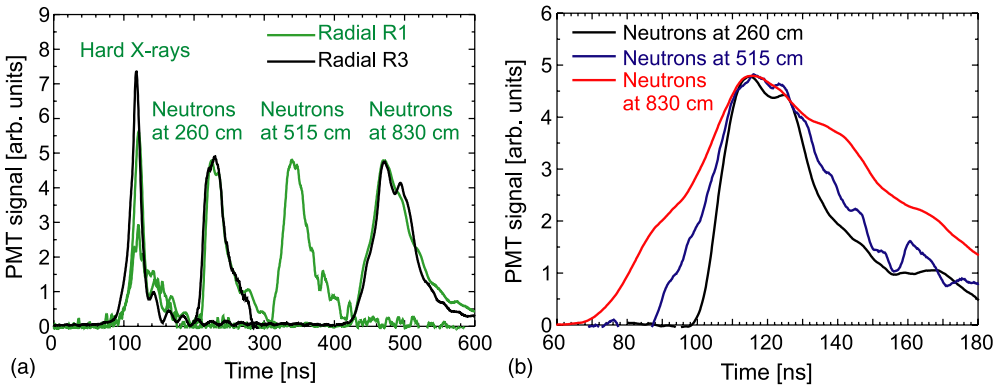

Figure 7. Neutron TOF signals on the side-on detectors in discharge No 090922, the neutron yield of 3×10^{10}. (*a*) Side-on TOF signals shifted by the TOF of x-rays. Neutron TOF detector (R3) at 515 cm was saturated in this particular shot. (*b*) Neutron TOF signals at various radial positions shifted by the TOF of 2.45 MeV neutrons.

3.4. Neutron energy spectra

Eleven fast plastic scintillators and photomultiplier tubes enabled the TOF analysis of fusion neutrons. In figure 7 we can see a typical example of TOF signals measured in the side-on direction. The first peak at 120 ns corresponds to hard x-rays above 200 keV. Other pulses represent neutron signals at various distances. It can be seen how the neutron signal shifts and broadens with increasing distance from the neutron source. It was caused by different velocities of neutrons. Qualitatively, we calculated neutron energy spectra from TOF signals by a Monte Carlo reconstruction [23, 35]. The neutron spectra which we received are displayed in figure 8. In the downstream direction (on the Z-pinch axis behind the cathode), the mean neutron energy was 2.60 ± 0.08 MeV with a 700 ± 200 keV width. Let us remind the reader here that the term 'downstream' means the direction of current flow (from the anode towards the cathode). In the side-on direction, the mean neutron energy was 2.40 ± 0.05 MeV and the width of the neutron spectra was 600 ± 150 keV. As regards neutron spectra from all 11 shots, average values were almost the same as in figure 8.

3.5. Energy distribution function of reacting deuterons

The knowledge of neutron energy spectra at different directions could provide important information about kinetic energies of deuterons which produce fusion neutrons. If we assume a binary reaction of a fast deuteron with a stationary one, the neutron energy E_n depends on the deuteron energy E_d and on the laboratory angle between the colliding fast deuteron and the outgoing neutron θ as

$$E_n(E_d, \theta) = E_d \frac{m_n}{2(m_n + m_{He})} \cdot \left(\cos\theta + \sqrt{\frac{m_{He}}{m_n}\left(1 + \frac{2Q}{E_d}\right) - \sin^2\theta} \right)^2, \quad (1)$$

where $Q \doteq 3.27$ MeV represents the energy released from the D(d,n)^{3}He fusion reaction, m_n is the neutron mass and m_{He} is the mass of helium $^3_2$He. If the deuteron energy (below 300 keV in our experiment) is much smaller than the fusion energy of 3.3 MeV, it is possible to simplify

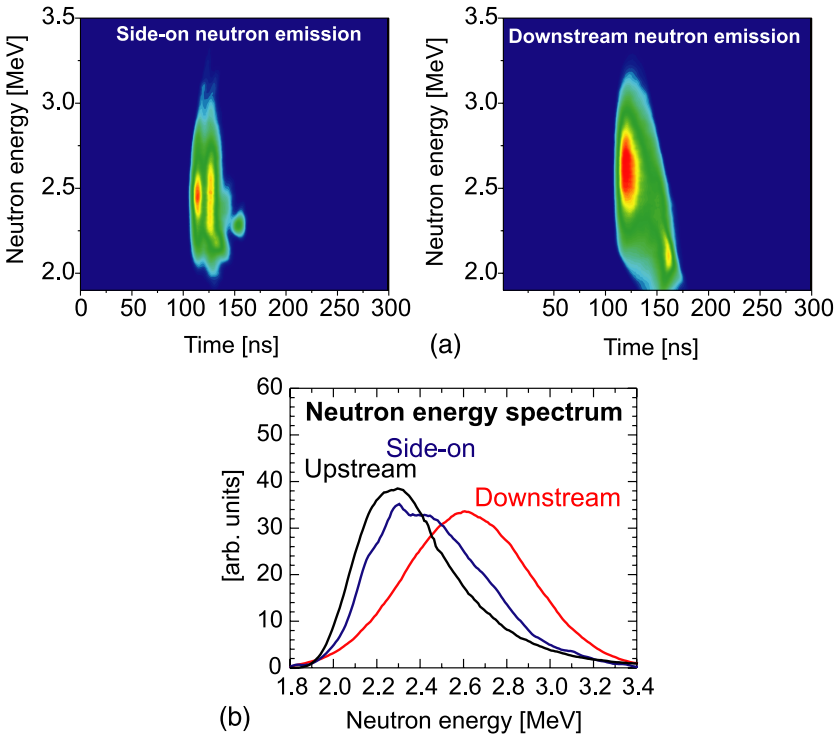

Figure 8. Neutron energy distribution functions in the side-on and end-on direction in shot No 090922, the neutron yield of 3×10^{10}. (*a*) Time-dependent. (*b*) Time-integrated.

the previous equation as

$$E_{\mathrm{n}}(E_{\mathrm{d}}, \theta) \doteq E_{\mathrm{d}} \frac{m_{\mathrm{n}}}{2(m_{\mathrm{n}} + m_{\mathrm{He}})} \cdot \left(\cos\theta + \sqrt{\frac{m_{\mathrm{He}}}{m_{\mathrm{n}}} \frac{2Q}{E_{\mathrm{d}}}} \right)^2 . \tag{2}$$

Then the component of deuteron kinetic energy in the direction of neutron detection can be calculated as

$$E_{\mathrm{d}} \cos^2\theta \doteq \frac{2(m_{\mathrm{n}} + m_{\mathrm{He}})}{m_{\mathrm{n}}} \cdot \left(\sqrt{E_{\mathrm{n}}} - \sqrt{\frac{m_{\mathrm{He}} Q}{m_{\mathrm{n}} + m_{\mathrm{He}}}} \right)^2 . \tag{3}$$

On the basis of the last equation, it was possible to transform the neutron spectra into energy distribution functions of deuterons which produced fusion neutrons. The distribution functions of the end-on and side-on component of kinetic energy obtained in the shot mentioned above can be seen in figure 9.

It can be clearly seen in figure 9 that most of the fusion neutrons were produced by deuterons with the kinetic energy component below 300 keV. It agrees with the fact that we observed the maximum neutron energy of about 3.2 MeV both in the side-on and end-on directions (see figure 8). As regards mean values, the mean axial component of the deuteron kinetic energy $\langle |E_{\parallel}| \rangle$ was 60 keV whereas the mean side-on component $\langle |E_{\perp}| \rangle$ was 40 keV. This means that the average kinetic energy of reacting deuterons was $\langle E_{\mathrm{d}} \rangle = \langle E_x + E_y + E_z \rangle = 2\langle |E_{\perp}| \rangle + \langle |E_{\parallel}| \rangle = 140\,\mathrm{keV} \doteq 150\,\mathrm{keV}$. From the deuteron energy spectra in figure 9, our Monte Carlo reconstruction estimated the downstream/upstream anisotropy of neutron flux as 1.1.

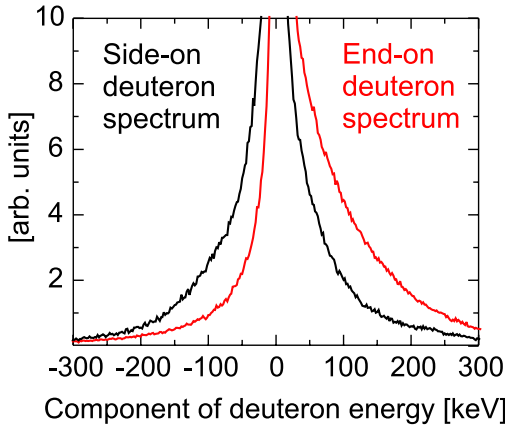

Figure 9. Distribution functions of kinetic energy components of reacting deuterons. The plus and minus signs of kinetic energy component reflect the direction of deuteron velocity. Shot No 090922, the neutron yield of 3×10^{10}.

4. Discussion

4.1. Mechanism of neutron production

On the basis of results presented above, we should be able to discuss neutron production mechanisms now. In this respect, two findings are of great importance. The first one concerns the time of neutron generation whereas the second one relates to neutron energy spectra.

4.1.1. Time of neutron emission. The first fundamental result is the time of neutron emission because most of the neutrons were not produced during the stagnation. Instead of that, they were produced during the global plasma expansion for quite a long period (35 ± 5 ns FWHM) after the soft x-ray peak. At this time, voltage peaks or a significant power input were not observed. However, the impedance was almost 0 despite the fact that the plasma was expanding. This means that the negative value of time-varying inductance $\dot{L}$ (which should be on the order of 0.1 Ω) was likely compensated by the plasma resistance R. The anomalously high resistance was reported on the Angara [14] and in PF [36, 37]. From the experimental point of view, the onset of microinstabilities just before neutron emission was clearly shown by Bernard *et al* with laser scattering in a plasma focus discharge [38]. With respect to PF, it seems worthy of remark that two neutron pulses were observed too. The first pulse was recorded during the so-called quiet phase of the stagnation and the second, i.e. the principal one, after the development of $m = 0$ instabilities [39].

As regards the temporal correlations in our experiment, the neutron and hard x-ray emission corresponded to peaks of the $\mathrm{d}I/\mathrm{d}t$ signal. This could be explained by the fact that charged particles accelerated to high energies carry a significant part of a fast changing electrical current. It follows that the acceleration mechanism is connected with global plasma dynamics and therefore it cannot be regarded as a 'secondary' process in plasma.

4.1.2. Neutron energy spectra. The second important topic in the discussion of neutron production mechanism is the analysis of measured neutron energies. As regards deuterium gas puff experiments on the S-300 generator, the mean neutron energy detected downstream was shifted from 2.45 MeV towards higher energies whereas the upstream neutron energy spectrum

had the maximum at about 2.2 MeV. That is why most fusion reactions were realized in the centre of the mass frame which was moving with respect to the laboratory frame of reference. One could therefore think that a deuteron beam was accelerated towards the cathode. However, a small shift from 2.5 MeV could have been either a result of a thermonuclear source moving towards the cathode or a consequence of an inhomogeneous density of target deuterons. And because the observed neutron emission anisotropy was too small to exclude a significant part of thermonuclear neutrons, the much more important result was the neutron energy spectrum measured in the side-on direction. What were the advantages that this direction brought to us? The first advantage of the side-on direction was a higher number of detectors in a row. The second advantage was a smaller influence of scattered neutrons because side-on diagnostic ports of 10 cm diameter and 1.5 m length were surrounded by water without significant mass distributed along the line of sight. On account of both these advantages side-on neutron energy spectra could be reconstructed more accurately. The important parameter regarding the side-on direction is a width of neutron energy spectra. In our experimental campaign, the broad width of side-on neutron energy spectra implied a high radial velocity of deuterons. If we assume the significant part of thermonuclear neutrons, the width of neutron energy spectrum would be given by $\triangle E_{\mathrm{n}}$ (keV) $= 82.5\sqrt{kT_{\mathrm{i}}[\mathrm{keV}]}$ (e.g. [40]). Therefore the 500 keV FWHM would require an unreasonably high temperature of 40 keV.

All these facts together, i.e. the time of neutron emission and the energy spectra, imply that most of the neutrons were not of thermonuclear origin. This could perhaps lead us to speak about the beam–target model. Nevertheless, the neutron production cannot be explained by a simple concept of the linear beam–target model because of a significant radial component of deuteron velocities. The observed spectra have to be explained by a broad angular dependence of the deuteron energy distribution function. The question of how deuterons are accelerated (e.g. if axially accelerated deuterons are bent by magnetic fields before they produce fusion neutrons or if the acceleration could occur also in the side-on direction) is being investigated and it is the subject of our future experiments.

4.2. Thermonuclear yield

Apparently, the thermonuclear mechanism was not dominant. In order to support such an observation, it is possible to calculate an expected thermonuclear yield from plasma parameters reached in our experiment. The thermonuclear yield is given by the equation

$$Y_{\mathrm{thermonuclear}} = \tfrac{1}{2} n_{\mathrm{i}}^2 \langle \sigma v \rangle_T \pi R^2 l \tau. \tag{4}$$

Plasma parameters are estimated in table 2. The ion temperature $T = 1$ keV was calculated from the energy input W_{input} and the total numbers of deuterons N_{total}.

For the plasma density $n_{\mathrm{i}} = 2 \times 10^{20}$ cm^{-3}, the plasma length $l = 2$ cm, the plasma radius $R = 1$ mm and the confinement time $\tau = 5$ ns, one obtains 2×10^8 thermonuclear neutrons. This is on the order of one per cent of the total neutron yield and on the order of the first neutron pulse observed immediately after the stagnation in figure 4(*b*).

4.3. Total energy of deuterons accelerated to fusion energies

The beam–target mechanism was identified in Z-pinches already in the 1950s. It was considered as a very pessimistic result with respect to fusion energy production. However, high neutron yields need to be studied and explained in more detail. This is the reason why it is interesting to calculate the number and energy of fast deuterons similarly to the way it was done for the Z-machine by Velikhovich *et al* in [19].

Table 2. Estimated plasma parameters.

Linear mass density	$m = 20\,\mu\mathrm{g\,cm^{-1}}$
Line density	$N = 6 \times 10^{18}$ deuterons $\mathrm{cm^{-1}}$
Length of plasma column	$l = 2\,\mathrm{cm}$
Total number of deuterons	$N_{\mathrm{total}} = Nl = 6 \times 10^{18} \cdot 2 \doteq 10^{19}$
Plasma radius during stagnation	$R \gtrsim 0.1\,\mathrm{cm}$
Ion density	$n_{\mathrm{i}} = N/\pi R^2 \approx 2 \times 10^{20}\,\mathrm{cm^{-3}}$
Energy input	$W_{\mathrm{input}} = \frac{1}{2}\int_0^{t_{\mathrm{imp}}} \dot{L} I^2 \mathrm{d}t \approx 8\,\mathrm{kJ}$
Temperature	$k(T_{\mathrm{i}} + T_{\mathrm{e}}) = \frac{2}{3} W_{\mathrm{input}}/N_{\mathrm{total}} \doteq 2\,\mathrm{keV}$
Ion temperature for $kT_{\mathrm{i}} = kT_{\mathrm{e}}$	$T = T_{\mathrm{i}} \doteq 1\,\mathrm{keV}$
D(d,n)^{3}He fusion reaction rate [41]	$\langle \sigma v \rangle_{T=1\,\mathrm{keV}} = 0.75 \times 10^{-22}\,\mathrm{cm^3}$
Confinement time	$\tau = 5\,\mathrm{ns}$
Ion–ion collision time	$\tau_{\mathrm{ii}} = 1/\nu_{\mathrm{ii}} = 0.4\,\mathrm{ns} \ll 5\,\mathrm{ns}$

The number of accelerated deuterons N_{d} depends on the neutron yield Y_{n}, the fusion cross-section $\sigma_{\mathrm{fusion}}(E_{\mathrm{d}})$, the deuteron density n_{d} and the path length l as

$$N_{\mathrm{d}} = \frac{Y_{\mathrm{n}}}{\sigma_{\mathrm{fusion}}(E_{\mathrm{d}}) n_{\mathrm{d}} l}. \tag{5}$$

In our experiment we measured the neutron yield $Y_{\mathrm{n}} \doteq 4 \times 10^{10}$ and the average energy of reacting deuterons $\langle E_{\mathrm{d}} \rangle \approx 150\,\mathrm{keV}$. Deuterons with such a kinetic energy have the fusion cross-section $\sigma_{\mathrm{fusion}}(150\,\mathrm{keV}) = 2.8 \times 10^{-30}\,\mathrm{m^{-2}}$ (see [42]).

During the main neutron emission, the plasma was expanded to the radius R greater than 5 mm. Because the line density of deuterons was $N = 6 \times 10^{18}$ deuterons $\mathrm{cm^{-1}}$, the upper value of ion density $n_{\mathrm{d}} = N/\pi R^2$ was $7.5 \times 10^{18}\,\mathrm{cm^{-3}}$. Further, one can estimate the path length of fast deuterons as $l \approx 3\,\mathrm{cm}$. For these values one obtains the number of accelerated deuterons $N_{\mathrm{d}} \approx 6 \times 10^{16}$. It is only a small fraction of the total number of deuterons $N_{\mathrm{total}} \doteq 10^{19}$ but it can be connected with a significant current and energy. The velocity of 150 keV deuterons is $3 \times 10^6\,\mathrm{m\,s^{-1}}$; therefore 6×10^{16} deuterons carry 30 kA current (cf with a 100–200 kA rise of the current during the hard x-ray and neutron emission). As regards the total energy of deuterons accelerated to fusion energies $W_{\mathrm{d}} = N_{\mathrm{d}} \langle E_{\mathrm{d}} \rangle$, it was above 1.5 kJ which is more than 15% of the energy input into a plasma during the implosion $W_{\mathrm{input}} = \frac{1}{2}\int_0^{t_{\mathrm{imp}}} \dot{L} I^2\,\mathrm{d}t$.

Since that is a surprisingly high efficiency, we wanted to be quite certain about this value. Firstly, the neutron yield was measured by several independent methods. Secondly, it was necessary to discuss the strong dependence of the fusion cross-section on the deuteron energy E_{d}. The total energy W_{d} is proportional to $\int f_{\mathrm{d}}(E_{\mathrm{d}}) E_{\mathrm{d}}/\sigma_{\mathrm{fusion}}(E_{\mathrm{d}})\,\mathrm{d}E_{\mathrm{d}}$. Since the ratio $E_{\mathrm{d}}/\sigma_{\mathrm{fusion}}(E_{\mathrm{d}})$ is the smallest exactly for $E_{\mathrm{d}} = 150\,\mathrm{keV}$, it means that we did a lower estimate of the total energy $W_{\mathrm{d}} \geqslant N_{\mathrm{n}} \langle E_{\mathrm{d}} \rangle / \sigma_{\mathrm{fusion}}(\langle E_{\mathrm{d}} \rangle) n_{\mathrm{d}} l$. Thirdly, the path length of 3 cm should be a credible estimation because such a distance is on the order of the anode–cathode separation. The length of 3 cm is also travelled by 150 keV deuterons during 10 ns which is the characteristic time of observed changes in neutron emission.

Finally, the most uncertain parameter was the density of target deuterons. We calculated the upper value of the density from the known linear mass density and from the observed diameter of globally expanding plasma which was detected by the streak camera. The density could have been higher than $7.5 \times 10^{18}\,\mathrm{cm^{-3}}$ in two cases. In the first case, the density could have been increased by secondary, local implosions; however, such implosions occurred usually before the main neutron pulse and were not observed during the peak of neutron emission. Moreover, there is a question of how to confine fast deuterons in a small, dense locality to

Table 3. Basic parameters and results achieved on Angara [14] and S-300 (this work).

	Angara	S-300
Current	2–3 MA	1.35–1.65 MA
Energy input W_{input}	20–30 kJ	<10 kJ
Linear mass density	5–50 μg cm^{-1} axial gradient of linear density	20 μg cm^{-1}
Anode–cathode separation	2–4 cm	1–2 cm
Initial diameter of solid gas puff	1.5–3.0 cm at cath. <6 cm at anode	4 cm
Implosion velocity	(4–5) $\times$ 10^5 m s^{-1}	(3–4) $\times$ 10^5 m s^{-1}
Zipper	35 ns	<10 ns
Time of neutron emission	after implosion after voltage drop	after implosion after voltage drop
Duration of neutron emission	40–50 ns FWHM	35 $\pm$ 5 ns FWHM
Peak neutron yield	$\approx 10^{12}$	6 $\times$ 10^{10}
FWHM of side-on energy spectrum	300 keV	600 $\pm$ 200 keV

achieve a sufficiently high pass length. In the second case, there might have remained a high density plasma near the Z-pinch axis even though the outer plasma shell expanded. We should exclude this possibility by laser probing in future experiments. Now we can argue that a dense region should be visible if it is heated by Coulomb collisions with a large number of fast deuterons. Further, it is possible to exclude neutron production outside the inter-electrode region: since the cathode was not hollow, the significant number of neutrons produced above the anode should cause a neutron emission anisotropy and a large shift of upstream neutron energies above 2.5 MeV. Such a result has, however, not been observed.

We conclude this discussion with an important argument about high efficiency of deuteron acceleration observed in PF and on the Angara Z-pinch. In PF devices, almost 10% conversion efficiency of stored energy into >25 keV deuterons is reported [43]. On the Angara [14], the neutron yield of 10^{12}, the deuteron energies of about 500 keV, the plasma (target) density of 10^{20} cm^{-3} with the path length of 4 cm imply the total number of deuterons of 4×10^{16} with an energy of 3 kJ. Since the energy input on the Angara was 20–30 kJ, the conversion efficiency to the energy of fast deuterons was also about 15%. Such a value is similar to the one achieved in our experiment with comparable electrical parameters.

4.4. Comparison with deuterium gas puffs on the Angara Z-pinch

The previous paragraph shows that the total numbers of accelerated deuterons are similar on the S-300 as well as on the Angara. At this point it seems proper to also provide a comparison of other parameters in both experiments (see table 3).

As regards the neutron emission, there were a lot of similarities. In both experiments, neutrons were produced for quite a long period after the implosion and after the voltage peak. The principal distinction between both experiments was the strong axial gradient of the linear gas puff density and the subsequent zipper. This difference could explain relatively high neutron yields achieved on the Angara Z-pinch and one order lower yield on the S-300 generator. On the one hand, the neutron yield on the S-300 was lower. But on the other hand, homogeneous plasma with the zipper below 10 ns and also the solid centre of the cathode are more convenient for the discussion of where and when deuterons are accelerated and where and when fusion neutrons are produced. The experiment at the Kurchatov Institute clearly showed that deuterons were accelerated in a lower density plasma during the global plasma

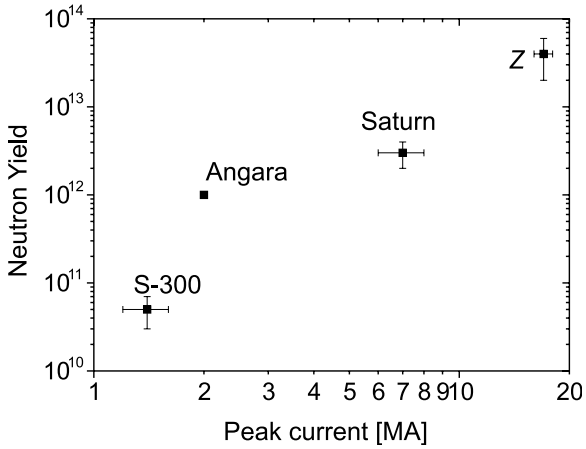

Figure 10. Neutron yields from deuterium gas puff Z-pinches [14, 16, 17].

expansion. Because of the axially homogeneous gas puff, also the density of a target plasma was low and subsequently the neutron yield was lower than on the Angara. On the Angara, deuterons were supposed to be accelerated also in a low density plasma. However, because of the axial gradient of plasma density, these deuterons could produce more neutrons in a dense plasma near the hollow cathode. We note that an analogical axial density gradient influences neutron yields in PF where a large number of neutrons are produced in a dense structure at the heel of the current sheath [6, 44, 45]).

4.5. Neutron yield scaling with current

To know the scaling law for a neutron yield is of crucial importance for future applications of Z-pinch facilities as sources of neutrons. This is why we present peak neutron yields achieved with deuterium gas puffs in figure 10.

The neutron yield from the S-300 is important for two reasons. Firstly, it makes it possible to enlarge the neutron scaling law for deuterium gas puffs below 2 MA currents. Secondly, it provides a reasonable comparison with experiments on Sandia's Saturn and Z-machine because all these gas puffs were more axially homogeneous than the one used on the Angara. If we leave out the neutron yield on the Angara, the total number of neutrons scales as $I^{2.9\pm0.2}$ in the 1.5–17 MA region. At 15 MA current, there is a hope of a large thermonuclear component. As regards the thermonuclear source, the neutron yield should theoretically increase as the fourth power of an electric current, i.e. $Y_n \propto n^2 \propto I^4$. If this I^4 law is valid above 20 MA currents, high current Z-pinches might be powerful sources of neutrons.

When thermonuclear fusion is concerned, the neutron yield, however, is not the most relevant parameter. A much more important value is the ratio between the energy released from fusion and the energy input into a plasma. In order to have this ratio high enough, it is not sufficient just to reach a high temperature, it means to accelerate a significant fraction of deuterons by elastic collisions in a Maxwellian plasma. It is also necessary to keep these fast deuterons in this high temperature region. (If deuterons escape a high temperature region, they are slowed down by cold deuterons usually without undergoing fusion reactions. Since $\sigma_{\text{fusion}}(E_\text{d})Q \ll \sigma_{\text{Coulomb}}(E_\text{d})E_\text{d}$, the fusion energy released is always smaller than the energy expended on the acceleration of fast deuterons. The only way to achieve the energy gain is to transfer the lost energy of fast deuterons to the acceleration of other deuterons in the same

plasma). In other words, it is necessary to have a sufficiently long time and enough high plasma density to produce a large number of fusion reactions. This condition has been expressed by the known Lawson criterion. At this stage we found it interesting to calculate the necessary density of Z-pinch plasmas from the Lawson criterion $n\tau \approx 10^{14}\,\mathrm{cm}^{-3}\,\mathrm{s}$.

Let us assume the confinement time of a gas puff Z-pinch $\tau = R/v_{T_i}$ on the order of 5 ns. Then the required density is about $2 \times 10^{22}\,\mathrm{cm}^{-3}$. This value is about 60 times higher than the plasma density achieved with 17 MA on the Z-machine [19]. If we consider the same character of implosions, i.e. the same value of dimensionless scaling parameter Π [46], then $n \propto m \propto I^2$ and the Lawson criterion could be achieved with 100 MA current drivers. It is a fairly high current. However, only a few experiments have been carried out with deuterium gas puffs. Therefore, more shots with multi-MA drivers and with various Z-pinch configurations (see, e.g., [46, 47] and references herein) are needed in order to study neutron production mechanism and to find out if it is possible to increase the plasma density and mainly the confinement time.

5. Conclusions

The neutron production and dynamics of deuterium gas puffs were studied on the S-300 generator. The axially homogeneous gas puff with the zipper below 10 ns and with the solid centre of the cathode was well suited for the discussion of where and when deuterons were accelerated and fusion neutrons were produced. The study of neutron emission was focused mainly on the estimation of neutron energies and neutron emission time, the anisotropy of neutron emission and the energy distribution of deuterons which produced fusion neutrons.

In the case of the linear mass density of $20\,\mu\mathrm{g\,cm}^{-1}$, the gas puff imploded onto the axis before the current peak at about 100 ns. The fusion neutrons were generated after the gas puff implosion during the global expansion of a plasma column. The neutron emission lasted on average 35 ± 5 ns. In the downstream direction (on the Z-pinch axis behind the cathode), the mean neutron energy was 2.6 ± 0.1 MeV. The side-on neutron energy spectra peaked at 2.40 ± 0.05 MeV with about 600 ± 150 keV FWHMs. The broad width of the side-on neutron spectra implied a high radial component of deuteron velocity. The average kinetic energy of fast deuterons, which produced fusion neutrons, was about 150 keV. Most of the fusion neutrons were produced by deuterons with the kinetic energy below 300 keV. At the current level of 1.5 MA, the peak neutron yield reached a value of 6×10^{10}. It is by one order higher in comparison with previous experiments with deuterated fibres, X-pinches, deuterated foams and imploding wire-arrays on the same current generator.

On the basis of the above-mentioned experimental data and observed plasma parameters, we concluded that, on the one hand, most of the neutrons were not of thermonuclear origin. On the other hand, however, the total energy of deuterons accelerated to fusion energies was above 1.5 kJ. It is more than 15% of the energy input into a plasma and therefore gas puff Z-pinches seem to be not only powerful sources of x-ray radiation but also efficient sources of $\approx$100 keV deuterons. Such a result is consistent with a high neutron yield observed on the Angara Z-pinch and PF with similar currents.

Acknowledgments

This research has been supported by project No LC528, No LA08024, No ME09087 of the Ministry of Education of the Czech Republic, by grant No SGS10/266/OHK3/3T/13 of the Grant Agency of the Czech Technical University in Prague, by the GACR grant No 202-08-P084 and by the IAEA Grant RC14817.

References

[1] Andrianov A M *et al* 1958 *Proc. 2nd United Nations Int. Conf. on Peaceful Uses of Atomic Energy, Geneva, 1958* vol 31 ed J H Martens *et al (United Nations, Geneva, Switzerland, 1958)* p 348
[2] Mather J W and Williams A H 1958 *Proc. 2nd United Nations Int. Conf. on Peaceful Uses of Atomic Energy, Geneva, 1958* vol 32 ed J H Martens *et al (United Nations, Geneva, Switzerland, 1958)* p 26
[3] Anderson O A *et al* 1958 *Phys. Rev.* **110** 1375
[4] Bernard A *et al* 1979 *Plasma Physics and Controlled Fusion Research (IAEA-CN-37), 7th IAEA Conf. on Plasma Physics and Controlled Nuclear Fusion (Innsbruck, Austria, 1978)* vol 2 (Vienna: IAEA) p 159
[5] Soto L 2005 *Plasma Phys. Control. Fusion* **47** A361
[6] Gribkov V A *et al* 2007 *J. Phys. D: Appl. Phys.* **40** 3592
[7] Lee S and Saw SH 2008 *J. Fusion Energy* **27** 292
[8] Kubes P *et al* 2009 *IEEE Trans. Plasma Sci.* **37** 2191
[9] Sethian J D *et al* 1987 *Phys. Rev. Lett.* **59** 892
[10] Sethian J *et al* 1991 *Workshop on Physics of Alternative Magnetic Confinement Schemes (Varenna, Italy, 1990)* ed S Ortolani and E Sindoni (Bologna, Italy: Editrice Compositori) p 511
[11] Scudder D W 1991 *Workshop on Physics of Alternative Magnetic Confinement Schemes (Varenna, Italy, 1990)* ed S Ortolani and E Sindoni (Bologna, Italy: Editrice Compositori) p 519
[12] Kies W *et al* 1991 *J. Appl. Phys.* **70** 7261
[13] Lebedev S *et al* 1998 *Phys.Plasmas* **5** 3366
[14] Batyunin A V *et al* 1990 *Sov. J. Plasma Phys.* **16** 597
[15] Smirnov V P 1991 *Plasma Phys. Control. Fusion* **33** 1697
[16] Spielman R B *et al* 1998 *D–D Fusion Experiments Using Fast Z Pinches* (Sandia National Laboratories) Rep. SAND98-0705
[17] Coverdale C A *et al* 2007 *Phys. Plasmas* **14** 022706
[18] Coverdale C A *et al* 2007 *Phys. Plasmas* **14** 056309
[19] Velikovich A L *et al* 2007 *Phys. Plasmas* **14** 022701
[20] Welch D R *et al* 2009 *Phys. Rev. Lett.* **103** 255002
[21] Scholz M *et al* 2001 *Nukleonika* **46** 35
[22] Krauz V I 2006 *Plasma Phys. Control. Fusion* **48** B221
[23] Klir D *et al* 2009 *IEEE Trans. Plasma Sci.* **37** 425
[24] Chernenko A S *et al* 1996 *11th Int. Conf. on High Power Particle Beams (Prague, Czech Republic)* vol 1 ed J Ullschmied (Prague: Academy of Science of Czech Republic) p 154
[25] Bakshaev Yu L *et al* 1996 *11th Int. Conf. on High Power Particle Beams (Prague, Czech Republic)* vol 2 ed J Ullschmied (Prague: Academy of Science of Czech Republic) p 962
[26] Klir D *et al* 2008 *Phys. Plasmas* **15** 032701
[27] Anan'ev S S *et al* 2008 *Plasma Phys. Rep.* **34** 574
[28] Waisman E M *et al* 2008 *Phys. Plasmas* **15** 042702
[29] Velyhan A *et al* 2006 *Phys. Scr.* **T123** 112
[30] Tiseanu I, Decker G and Kies W 1996 *Nucl. Instrum. Methods Phys. Res.* A **373** 73
[31] Tiseanu I and Craciunescu I 1996 *Nucl. Sci. Eng.* **122** 384
[32] Klir D *et al* 2006 *Phys. Scr.* **T123** 116
[33] Bakshaev Yu B *et al* 2006 *Plasma Phys. Rep.* **32** 531
[34] Akunets A A *et al* 2009 *Eur. Phys. J.* D **54** 499
[35] Řezáč K *et al* 2006 *Czech J. Phys.* **56** B357
[36] Decker G *et al* 1983 *Phys. Fluids* **26** 571
[37] Bernard A 1978 *Atomkernenergie* **32** 73
[38] Bernard A *et al* 1975 *Phys. Fluids* **18** 180
[39] Schmidt H *et al* 2006 *IEEE Trans. Plasma Sci.* **34** 2363
[40] Wolle B 1999 *Phys. Rep.* **312** 1
[41] Huba J D 2009 *NRL Plasma Formulary* (Washinghton DC: Naval Research Laboratory) p 45
[42] Chadwick M B *et al* 2006 *Nucl. Data Sheets* **107** 2931
[43] Stygar W, Gerdin G, Venneri F and Mandrekas J 1982 *Nucl. Fusion* **22** 1161
[44] Sadowski M J and Malinowska A 2006 *Czech. J. Phys.* **56** B364
[45] Kubes P *et al* 2010 *IEEE Trans. Plasma Sci.* **38** 672
[46] Ryutov D D, Derzon M S and Matzen M K 2000 *Rev. Mod. Phys.* **72** 167
[47] Slutz S A *et al* 2010 *Phys. Plasmas* **17** 056303